

Observable Effects of Dust Formation in Dynamic Atmospheres of M-type Mira Variables

M.J. Ireland^{1*}, M. Scholz^{1,2}

¹*School of Physics, University of Sydney NSW 2006, Australia*

²*Institut für Theoretische Astrophysik der Universität Heidelberg, Albert-Ueberle-Str.2, 69120 Heidelberg, Germany*

7 July 2018

ABSTRACT

The formation of dust with temperature-dependent non-grey opacity is considered in a series of self-consistent model atmospheres at different phases of an O-rich Mira variable of mass $1.2 M_{\odot}$. Photometric and interferometric properties of these models are predicted under different physical assumptions regarding the dust formation. The iron content of the initial silicate that forms and the availability of grain nuclei are found to be critical parameters that affect the observable properties. In particular, parameters were found where dust would form at 2-3 times the average continuum photospheric radius. This work provides a consistent physical explanation for the larger apparent size of Mira variables at wavelengths shorter than $1 \mu\text{m}$ than that predicted by fundamental-mode pulsation models.

Key words: techniques: interferometric – stars: variables: Miras – stars: AGB and post-AGB

1 INTRODUCTION

Dust shells around Mira variables often dominate the mid- and far-infrared regions of their spectra and strongly influence the observed brightness distributions of their stellar and circumstellar material. In contrast to C-type Miras for which substantial theoretical progress has been made in recent years (e.g. Helling et al. 2000; Schirrmacher et al. 2003; Höfner et al. 2003; Gautschy-Loidl et al. 2004), for oxygen-rich M-type Miras the physical conditions and the geometric region of formation of dust grains is poorly understood.

This situation is first of all due to the much more complex physics of formation of typical dust grains, which may contain metal oxides such as corundum (Al_2O_3), silicates or even solid iron (Gail 2003). These heterogenous grains form around nuclei that are in general composed of different compounds again, such as TiO_2 (Jeong et al. 2003). Furthermore, in order to understand the occurrence of dust in an M-type Mira, the formation of grains has to be studied within the physical environment of the time-dependent dynamic atmosphere of the pulsating star. Interferometric observations indicate that the inner radii of dust shells may be as small as 2 to 4 stellar radii where the stellar radius refers to the position of the continuum-forming layers (e.g. Danchi et al. 1994; Danchi & Bester 1995; Lopez et al. 1997; Monnier et al. 2004; Ireland et al. 2004d, 2005). This is well within the upper regions of the stellar atmosphere in which typical molecular features of

the stellar spectrum are formed (cf. Hofmann et al. 1998; Tej et al. 2003a,b; Ohnaka 2004; Perrin et al. 2004; Ohnaka et al. 2005)

So far existing dynamic model atmospheres of M-type Mira stars either are dust-free (e.g. Hofmann et al. 1998; Woitke et al. 1999; Höfner et al. 2003), or they use grey, composition independent dust opacities (e.g. Winters et al. 2000; Jeong et al. 2003). Bedding et al. (2001) studied schematically the conditions of dust formations in the models of Hofmann et al. (1998) and concluded that corundum and silicate grains are likely to occur, depending on the phase of pulsation, in the upper layers of the star's atmosphere. However, only a small number of observable features of a small number of models were considered, with a very simple opacity treatment.

In this paper we investigate the formation of dust in a series of dynamic models of a Mira variable, and discuss which observable effects would result from different physical assumptions regarding the dust formation. In particular, we focus on effects of non-grey opacities of silicate dust with a variable Fe content and the effect of grain size on observable properties. As heterogenous O-rich dust formation is complex, our approximations are designed to be most valid for only the innermost dust that has a significant influence on observable properties. We aim to parametrize uncertainties in this first significant dust formation with the smallest number of physical free parameters.

2 SIMPLE DUST MODELS

In this section, we will describe the procedure we used to calculate absorption and scattering coefficients for silicate dust. We will then discuss the degree of validity of this procedure for the physics ap-

* Present Address: Division of Geological and Planetary Sciences, Mail Code 150-21, California Institute of Technology, 1200 East California Boulevard, Pasadena, CA 91125, USA; mireland@gps.caltech.edu

plicable to Mira atmospheres, the way in which corundum dust is added to the models and finally the definition of the dust types used in the models.

The properties of a given dust type are considered to be wholly determined by the dust temperature T_d and the gas pressure P . T_d is found by solving the equation of radiative equilibrium:

$$\int \kappa_\nu J_\nu d\nu = \int \kappa_\nu B_\nu d\nu \quad (1)$$

where J_ν is the mean intensity, $B_\nu = B_\nu(T_d)$ is the Planck function, and $\kappa_\nu = \kappa_\nu(T_d, P)$ is the dust absorption coefficient in the layer with local dust temperature T_d and local gas pressure P . The mean intensity is found iteratively in the modelling procedure described in Section 3. The gas temperature T_g does not enter in to this equation because the dust energy exchange with the gas is negligible compared to the dust energy exchange with the radiation field (e.g. see Appendix D of Gauger et al. 1990).

2.1 Silicate Dust Properties

We assume that the silicate that condenses first is olivine, $\text{Mg}_{2x}\text{Fe}_{2-2x}\text{SiO}_4$, and use a simplified version of the non-equilibrium treatment of Gail & Sedlmayr (1999) to determine the condensation fraction of Si, f_{Si} , and the composition parameter x . f_{Si} is assumed to follow the following simple relationship:

$$f_{\text{Si}} = \begin{cases} 0 & T_d > 1240 + 46 \log P \\ 0.25 & T_d < 1215 + 46 \log P \\ \frac{1240 + 46 \log P - T_d}{100} & \text{Otherwise} \end{cases} \quad (2)$$

The stability limit of silicate in this equation comes from a linear fit to the stability limit for forsterite shown in Gail (2003) for solar metallicity. The upper limit for Si condensation of 0.25 was chosen somewhat arbitrarily, so that there was not unrealistic grain growth in outer atmospheric layers, where low gas pressures mean that the silicate condensation fraction is far from equilibrium. The dependence of the olivine stability temperature on x is neglected in Equation 2. However, its inclusion would not cause any significant changes to this paper, as the lowest value of x considered is 0.775, where the difference in stability temperature of the olivine from pure forsterite is only 30 K. More sophistication was not warranted in this relationship because the true equilibrium condensation fraction is a function of both T_d and T_g , and the system is not in general close to chemical equilibrium.

In practice, the Si condensation fraction f_{Si} is determined by the functions $x(f_{\text{Si}})$ and $T_d(x)$, given that the opacity of silicate around $1 \mu\text{m}$ is a very strong function of the composition parameter x . In equilibrium condensation calculations, $x \approx 1$ for the initial condensate as it is energetically more favorable in the bulk solid to have Mg rather than Fe anions. However, the pulsating atmosphere of a Mira variable is certainly not one where chemical equilibrium considerations apply. To find $x(f_{\text{Si}})$, we consider x to be defined by the conditions during rapid grain growth, approximate $K_p = 0$ in Equations (55-57) of Gail & Sedlmayr (1999) (a reasonable approximation as seen by the near-constant $x(T_d)$ functions in Figure 3 of that paper) and assume that the grain has the same composition x throughout. This gives:

$$x = \frac{p_{\text{Mg}}}{p_{\text{Fe}} + p_{\text{Mg}}} + \frac{\alpha}{2} \sqrt{\frac{m_{\text{SiO}} p_{\text{Mg}}}{m_{\text{Mg}} p_{\text{SiO}}}} \quad (3)$$

$$= \frac{\epsilon_{\text{Mg}} - 2x f_{\text{Si}} \epsilon_{\text{Si}}}{\epsilon_{\text{Mg}} + \epsilon_{\text{Fe}} - 2f_{\text{Si}} \epsilon_{\text{Si}}} + \frac{\alpha}{2} \sqrt{\frac{m_{\text{SiO}}}{m_{\text{Mg}}} \frac{\epsilon_{\text{Mg}} - 2x f_{\text{Si}} \epsilon_{\text{Si}}}{\epsilon_{\text{Si}} (1 - f_{\text{Si}})}} \quad (4)$$

Here p_{Mg} and p_{Fe} are the partial pressures of Mg and Fe left in the gas mixture, and m_{SiO} and m_{Mg} are the masses of an SiO molecule and an Mg atom respectively. Equation 4 is solved for x , which is limited to be less than or equal to 1. The elemental abundances ϵ come from Palme et al. (1981), for consistency with the modelling code. α is the ratio of the exchange coefficient for Mg and Fe ions to the sticking coefficient for SiO molecules.

For α greater than or equal to 1, the assumption that the grain has the same composition x throughout is justified if the diffusion timescale for Fe and Mg anions is small compared to the timescale for grain growth. From the discussion in Section 5.2 of Gail (2003), this is the case for olivine at dust temperatures above about 900 K and grain sizes less than about $0.1 \mu\text{m}$. However, for small values of α , the value of x calculated using Equation 4 will only be the composition of newly deposited material on a growing grain, and not the composition of the whole grain. During grain destruction, Equation 4 does not accurately describe the grain composition, but the general property predicted by this equation that x will increase as the grain evaporates is consistent with experimental studies (Ozawa & Nagahara 2000).

In practice, Equation 4 is a good approximation for x during initial condensation or a phase of rapid grain growth if α is greater than about 1.0. In other cases, it represents a simple parameterization of x that includes an appropriate decrease in x as Mg is depleted from the gas phase.

In forming Equation 4 from Equation 57 of Gail & Sedlmayr (1999), it was assumed that $\alpha_{\text{Mg}} v_{\text{Mg}} = \alpha_{\text{Fe}} v_{\text{Fe}}$, the same assumption used to create Figure 3 of Gail & Sedlmayr (1999). In this relationship, the α_{Mg} and α_{Fe} parameters are sticking coefficients and the v parameters are thermal velocities. This is a necessary assumption given the lack of experimental data for olivine sticking coefficients with intermediate values of x .

Absorption and scattering coefficients are scaled as in the Rayleigh limit, where at a constant condensation fraction the absorption coefficient is independent of grain radius, and the scattering coefficient is proportional to the cube of the grain radius, a . The grain radius relates to the Si condensation fraction f_{Si} and the number of available nuclei per hydrogen atom N_{nuc} by the formula:

$$a = \left(\frac{3\epsilon_{\text{Si}} V_0}{4\pi f_{\text{Si}} N_{\text{nuc}}} \right)^{1/3} \quad (5)$$

Here ϵ_{Si} is the abundance of Si at solar metallicity, and V_0 is the volume of the monomer, taken to be $7.5 \times 10^{-23} \text{ cm}^3$. The optical constants of the olivine with $x = 0.5$ are taken from Dorschner et al. (1995), and those for forsterite with $x = 1.0$ taken from Jäger et al. (2003). These constants are used to derive $\kappa_{0.5}$, $\sigma_{0.5}$, $\kappa_{1.0}$ and $\sigma_{1.0}$ in the Rayleigh limit for 30 nm grains, with the subscripts 0.5 and 1.0 representing x for the olivine. The absorption and scattering coefficients for the olivine are then approximated by a simple interpolation:

$$\kappa_{\text{ol}} = f_{\text{Si}}((2 - 2x)\kappa_{0.5} + (2x - 1)\kappa_{1.0}) \quad (6)$$

$$\sigma_{\text{ol}} = \frac{2.6 \times 10^{-11}}{N_{\text{nuc}}} f_{\text{Si}}^2((2 - 2x)\sigma_{0.5} + (2x - 1)\sigma_{1.0}) \quad (7)$$

2.2 Dust Formation in a Typical Mira Atmosphere

In the above parameterisation of absorption and scattering coefficients, four important aspects of grain growth and destruction were not discussed: dust nucleation, the approximation of using a single grain radius a , the timescale of grain growth and destruction

compared to the pulsation timescale and the possibilities for further grain growth beyond $f_{\text{Si}} = 0.25$. We will discuss these one at a time, with specific reference to the physics of a Mira atmosphere.

The first stage of dust formation is the nucleation of seeds in a super-saturated gas. The number of seed nuclei available for grain growth determines the grain size. In the detailed nucleation discussion of Jeong et al. (2003), the seed nuclei are found to form from TiO_2 . The nucleation rate is a complicated function of temperature and pressure: at a typical Mira atmosphere dust formation pressure of 0.1 dyn/cm^{-2} , the TiO_2 nucleation rate increases from 10^{-29} to 10^{-17} per H atom per second as temperature decreases from 1200 to 1150 K. This relationship has significant uncertainties, as it is based on ab initio calculations from Jeong et al. (2000) which predicts an erroneous zero-point energy of TiO_2 by 0.73 eV or 5%, much larger than experimental errors (compare Table 2 of that paper with Balducci et al. (1985)). If one assumes all energies are erroneous by this relative amount, then errors in nucleation temperatures of the order of 50 K would be expected. Given these difficulties, we will consider that grain nucleation is complete when the growth of dominant dust components begins, and leave the number of grain nuclei per H atom N_{nuc} a free parameter in our models.

By separating nucleation and growth in this artificial way, we make the approximation that all dust grains in a single atmospheric layer are the same size. The effect of this dust on absorption and scattering is only equivalent to a distribution of particle sizes in the Rayleigh limit when the grain radius $a \ll \lambda$, a condition always met for the dust types and wavelengths considered here. This approximation is also more desirable than fixing a single particle size distribution at all atmospheric layers, as that approach doesn't include the increase in scattering coefficients with increasing grain radius.

As material cooling behind a shock in a Mira atmosphere moves outwards, the dust condensation fraction given by Equation 2 rapidly increases as the central luminosity decreases near minimum and the radiation field becomes increasingly geometrically diluted. For the dust treatment here (assuming f_{Si} is a function of the instantaneous variables T_d and P), the grain growth must be rapid compared to the dynamical timescale. According to Gail & Sedlmayr (1999), the limiting factor in the growth rate of olivine is the deposition of an SiO molecule on the grain surface. Considering a super-saturated gas mixture at 1100 K with an assumed sticking coefficient for SiO of 0.1, the rate of grain growth is greater than 10 nm in 0.1 cycles (3×10^6 s) whenever $\log(P) > -2.22$. Therefore, we shall be cautious in interpreting any dynamical grain growth and destruction effects that occur at $\log(P) < -2.22$.

At dust temperatures where olivine has mostly condensed, there are a variety of possibilities for further dust condensation, including quartz, and solid iron. In a non-equilibrium scenario, further model condensation will depend on the initial choice of α , as well as other unknown parameters. Note that at the near-maximum model phases, $f_{\text{Si}} = 0.25$ is never reached in the outer layers (near the arbitrary $5 R_p$ model surface: see Section 3), and the low gas pressures would mean that any growth would be slow compared to the dynamical timescale.

2.3 Addition of Corundum

It has been suggested (e.g. Maldoni et al. 2005; Egan & Sloan 2001) that corundum (Al_2O_3) plays a significant role in radiative transfer processes in O-rich AGB stars. This is due to the clear need for opacity in the 12-15 μm range when fitting models to ob-

served spectral energy distributions. However, physical models of Mira atmospheres with realistic gas densities (e.g. Bedding et al. 2001) have previously shown that the opacity of corundum and the abundance of Al are not high enough to have a significant effect on observed spectra. Therefore, we will re-examine the effects of corundum in this paper.

The difficulty in modelling the growth of corundum grains is that nucleation and growth will certainly be simultaneous, due to the high corundum stability temperature. In this paper we are not concerned about the details of this process, but attempt to allow corundum to have the maximum plausible effect on the radiative transfer.

We have taken the stability limit for corundum at solar metallicity from Gail (2003), fitting a function linear in $\log P$ for $-4 < \log P < 0$. For corundum dust only, the Al condensation fraction f_{Al} is given by:

$$f_{\text{Al}} = \begin{cases} 0 & T_d > 1600 + 60 \log P \\ 1.0 & T_d < 1500 + 60 \log P \\ \frac{1600 + 60 \log P - T_d}{100} & \text{Otherwise} \end{cases} \quad (8)$$

The dust temperature T_d is found using Equation 1, with the optical constants of corundum taken from Koike et al. (1995) and the Rayleigh limit again assumed. For silicate dust, corundum absorption and scattering coefficients are also added to those of the silicates, with $f_{\text{Al}} = f_{\text{Si}}$. This procedure is designed to approximate the effect of heterogeneous grains with a corundum core and a silicate mantle. Any pure corundum grains would have a much lower T_d in the outer atmosphere than a grain that includes silicate with $x < 1$, and therefore would not be significant if heterogeneous grains are also present.

Possibly, the optical constants of Koike et al. (1995) overestimate the absorption in the near-infrared region of the spectrum, given that their optical constants k for amorphous corundum are high when compared to thin-film alumina (Harris 1955) or crystalline corundum (Harman et al. 1994). However, a lower value for k could not cause a $> 20\%$ change in the calculated stability radius of corundum, as the gas is already becoming optically-thick in the mid-IR at the calculated stability radius due to molecular absorption, meaning that the dust can not have a significantly lower temperature than the gas. Furthermore, a smaller stability radius for corundum would place it at radii smaller than those at which successful nucleation could occur (cf. Section 2.2).

2.4 Model Dust Types

The dust types considered in this paper are given in Table 1. Dust types A and B have $\alpha = 1.0$, and represent olivine that will form pure forsterite initially in an outward-moving gas packet, before becoming enriched by Fe as the partial pressure of Mg decreases at $f \approx 0.15$. A higher value of α would give dust where Mg condenses more fully before the addition of Fe to the olivine. The difference between dust A and B is the number of grain nuclei, and hence the grain size: dust A will have dust grains $\sqrt[3]{10}$ times larger than dust B. Dust C is a dust where some the initial condensate contains an appreciable amount of Fe ($x = 0.93$), giving a higher absorption coefficient at wavelengths from 1 to 4 μm , where the bulk of the stellar flux is emitted.

Dust type D, with corundum only, can be thought of as the dust that would exist if $\alpha < 0.4$, as in this case silicates do not condense in our models. The effect of corundum on radiative transfer processes is at roughly the maximum plausible with the chosen

Table 1. Dust types considered in this paper. Columns are: Code used in this paper; Types of dust included (Olivine and Corundum); log of the number of grain nuclei per H nucleus; and α , the ratio of the exchange coefficient for Mg and Fe to the sticking coefficient for SiO (see text).

| Dust Code | Dust Types | $\log(N_{\text{nuc}})$ | α |
|-----------|------------|------------------------|----------|
| A | OI | -13.3 | 1.0 |
| B | OI | -12.3 | 1.0 |
| C | OI | -12.3 | 0.63 |
| D | Cor | -13 | - |

value of $N_{\text{nuc}} = 10^{-13}$, because much larger grains could not grow in an outward-moving gas packet even with sticking coefficients of 1.0.

3 MODELLING DETAILS AND RESULTS

The atmospheric models used in this study are based on model series of Hofmann et al. (1998), supplemented by models of Tej et al. (2003b) and Ireland et al. (2004b,c). These are non-grey dynamic model atmospheres for an M-type Mira variable with fundamental-mode period 332 days, mass $1.2 M_{\odot}$ (M series; P series: $1.0 M_{\odot}$) and solar metallicity. The luminosity L_p and Rosseland radius R_p of the non-pulsating parent star are $3470 L_{\odot}$ and $260 R_{\odot}$ (M series; P series: $241 R_{\odot}$). We refer to Hofmann et al. (1998) for essential details of model construction. In particular, these are self-excited models that were allowed to relax over a very large number of cycles. Pulsation is not strictly periodic, and the successive cycles that were studied in detail by Hofmann et al. (1998) and Ireland et al. (2004b, c) were so chosen that cycles of the M and P series with different characteristics are included. Phases assigned to these models (Ireland 2004b, c) are based on a reasonably chosen mean zero point, and the individual phase of a model of a specific cycle always refers to this zero point. The hydrodynamic models were calculated with dust-free grey opacities, and a non-grey temperature stratification of the atmospheric layers was then obtained in a second step by solving the radiative-equilibrium equation (i.e. equation 1 with $B_{\nu}(T_g)$, gas absorption coefficient $\kappa_{\nu,g}(T_g, P)$, gas temperature T_g) with dust-free non-grey opacities (see Hofmann et al. 1998), retaining the gas-pressure stratification of the hydrodynamic model.

During pulsation, the position of the continuum-forming layers oscillates around R_p with an amplitude of $\pm 30\%$. The parameters for the models at the individual phases considered here are shown in Table 2, reproduced from Ireland et al. (2004b). For comparisons with observations at specific visual phases, 0.12 will be added to ϕ_{vis} in Table 2 (Ireland et al. 2004b).

Using these dust-free models as a starting point, the dust types as described in Section 2 were added to the models, and the temperature profile, spectra and intensity profiles re-calculated. The new gas-temperature T_g and the dust-temperature T_d stratifications were obtained by iteration, that is, radiative equilibrium was enforced for both components (gas and dust) in each iteration step for obtaining for the next step new values of gas and dust temperatures, of gas and dust absorption coefficients, and of mean intensities J_{ν} (cf. comments on dust type D2 in Bedding et al. 2001). Note that scattering is approximated as being isotropic and coherent in these models and, hence, does not appear explicitly in Equation 1. Note also, that radiative acceleration does not become sufficiently large in the dusty models for generating a dust-driven wind, so that re-

Table 2. Parameters of M series Mira models. The columns: visual phase ϕ_{vis} ; luminosity L ; $1.04 \mu\text{m}$ near-continuum radius $R_{1.04}$; and the effective temperature $T_{1.04}$ corresponding to $R_{1.04}$.

| Model | ϕ_{vis}^1 | L (L_{\odot}) | $R_{1.04}$ (R_p) | $T_{1.04}$ (K) |
|-------|----------------|------------------------|-------------------------|-------------------|
| M05 | 0+0.49 | 1470 | 0.84 | 2420 |
| M06n | 0+0.60 | 2430 | 0.78 | 2860 |
| M08 | 0+0.77 | 4780 | 0.81 | 3320 |
| M09n | 0+0.89 | 5060 | 1.03 | 2970 |
| M10 | 1+0.02 | 4910 | 1.18 | 2760 |
| M11n | 1+0.11 | 4360 | 1.21 | 2640 |
| M12n | 1+0.21 | 3470 | 1.18 | 2540 |
| M12 | 1+0.27 | 2990 | 1.12 | 2500 |
| M14n | 1+0.40 | 1670 | 0.91 | 2400 |
| M15 | 1+0.48 | 1720 | 0.83 | 2530 |
| M16n | 1+0.60 | 2460 | 0.77 | 2860 |
| M18 | 1+0.75 | 4840 | 0.81 | 3310 |
| M18n | 1+0.84 | 4980 | 1.00 | 3010 |
| M19n | 1+0.90 | 5070 | 1.09 | 2900 |
| M20 | 2+0.05 | 4550 | 1.20 | 2680 |
| M21n | 2+0.10 | 4120 | 1.21 | 2610 |
| M22 | 2+0.25 | 2850 | 1.10 | 2490 |
| M23n | 2+0.30 | 2350 | 1.03 | 2460 |
| M24n | 2+0.40 | 1540 | 0.87 | 2410 |
| M25n | 2+0.50 | 2250 | 0.79 | 2780 |

¹ 0.12 should be added to these phases to give a more accurate model phase. See Ireland et al. (2004b).

taining the gas-pressure stratification of the original grey dynamical model is a reasonable approximation.

The M series was chosen over the P series for this study because approximations at $3-5 R_p$ caused unrealistic density jumps with respect to time in the P series. These approximations included coarse gridding in the dynamical models, and an artificial density-gradient cutoff that had been enforced in the outer layers at some phases/cycles for computational reasons (non-physical density discontinuity at the $5 R_p$ model surface). The M series models considered here have no artificial cutoff applied, and have a fine enough gridding of the dynamical models at $3-5 R_p$ to produce no unrealistic effects.

The P and M model series are meant to describe typical Miras like *o* Cet or R Leo. Comparison with observations of both stars (Hofmann et al. 2001; Ireland et al. 2004a,b; Woodruff et al. 2004; Fedele et al. 2005) show satisfactory agreement of observed and predicted features, but various deviations are also obvious from the discussion of Ireland et al. (2004c). We may check in this study whether some of these deviations are due to the omission of dust in the original models. Note that the mean-opacity treatment of strong water bands cools the outer layers too much and back-warms the continuum photosphere, as evident in the spectra of Tej et al. (2003b). If the forest of water lines were treated correctly in the models, one would expect the modelled water-bands to become less deep and the continuum (J-K) colour to become redder. This would give colour temperatures slightly lower than *o* Cet or R Leo. For this reason, we expect that realistic dust formation in these models would be at least as efficient as in *o* Cet or R Leo.

Figure 1 shows the dust stability radii for all dust types in Table 1. The dotted line shows the location of a single mass zone (the upper mass zone in Figure 2 of Hofmann et al. (1998)), giving an indication of the dynamics of the atmosphere. For dust types A, B and D, by far the largest rate of grain growth occurs just after initial

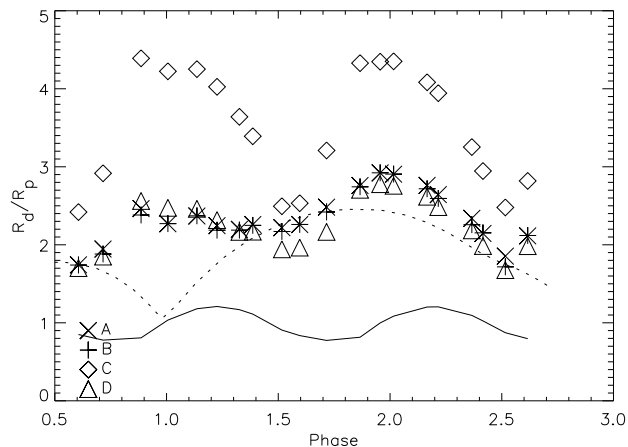


Figure 1. Model dust formation radii plotted against phase (0.12 has been added to the Table 2 phases - see text) for the four dust types considered here. The solid line shows the position where the dust-free near-continuum radius $R_{1.04}$, and the dotted line shows the position of a single mass zone as a function of phase.

grain formation, so it is in the initial stages of grain growth where it is most important to examine our assumption of dust condensation responding instantly to changes in the radiation field. For the mass zone shown in Figure 1 and zones immediately above it, the largest rate of grain growth occurs between phases 1.3 and 1.7, where the material crosses the dust stability radius. At these phases the material behind a strong shock (which reaches $2.75R_p$ at phase 1.7) is cooling as it moves outwards. As the material crosses the dust stability radius for dust types A and B at these phases, $\log(P)$ is between -1.9 and -1.7 with a local pressure scale height of $0.3R_p$. At these pressures, dust growth is sufficiently rapid according to the considerations of Section 2. However, this condition is not well-satisfied at all phases, so the details of the phase-dependence of the dust condensation radii should not be considered a reliable prediction of these simple models.

The total optical depth of the dust at $1.04 \mu\text{m}$ as a function of phase is shown in Figure 3 for all dust types. The large optical depths for dust type A are due to scattering by grains that reach a maximum radius of 96 nm in the outer layers, and reach 80 nm radius rapidly after condensation while x is equal to 1.0. The optical-depths for dust types A and B imply that the $1.04 \mu\text{m}$ near-continuum wavelength may not be a good window for interferometrically observing the continuum-forming photosphere as suggested by e.g. Jacob & Scholz (2002). As scattering opacity scales as λ^{-4} in the Rayleigh limit, the J and H band windows are not nearly as affected by the presence of these dust types as the $1.04 \mu\text{m}$ window. It is clear that dust types C and D have would have only a minimal effect at this wavelength.

The C-rich dust models of Höfner et al. (2003), at nearly twice the luminosity of the M-series considered here, have a large radiative acceleration of the dust grains which significantly modifies the dynamic stratification of these models. At the $5 R_p$ surface of the models considered here, the radiative acceleration ranges from 0.08 to 0.29 times gravitational acceleration for dust A. This range of values is smaller for all other dust types or for radii less than $5 R_p$. This is easily understandable as dust only forms within $5 R_p$ if the dust has a low opacity between 1 and 4 microns, where the bulk of the stellar flux is emitted. Therefore, we do not expect radiative acceleration of dust grains to play a highly significant role in the

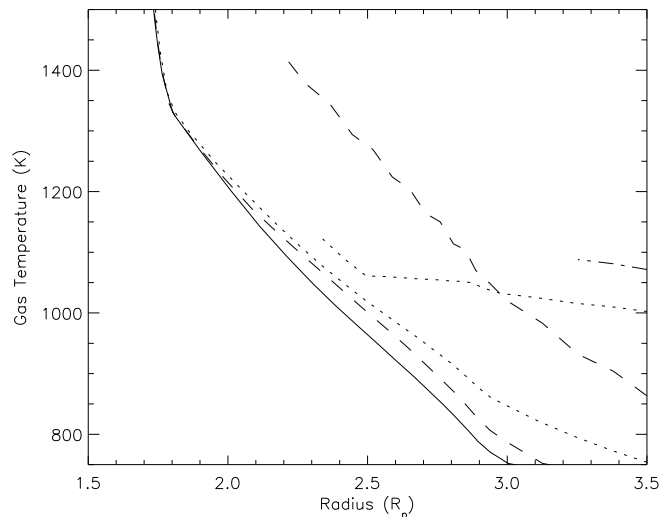


Figure 2. Gas temperatures (lower lines) and dust temperatures (upper truncated lines) for the M22 models. The solid line is for the dust-free model, the dotted line dust A, the dashed line dust D and the dot-dashed line dust C. Dust type B is nearly indistinguishable from the dotted line and the gas temperature for dust C is nearly indistinguishable from the solid line. The dust-free near-continuum radius $R_{1.04}$ for this model is $1.1 R_p$.

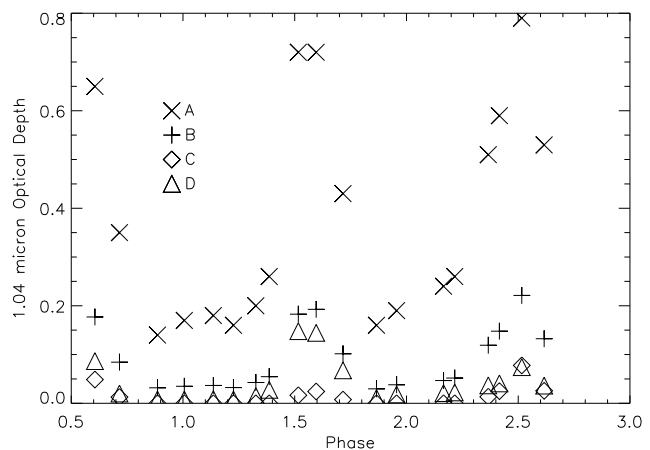


Figure 3. Total optical depths at $1.04 \mu\text{m}$ as a function of phase for the four dust types.

dynamic stratification of a typical Mira variable of luminosity less than about $5000L_\odot$ within 5 parent-star radii. However, beyond the surface of the models presented here radiative acceleration is expected to become significant as long as it is possible for the near-infrared opacity of the dust to increase with further Fe condensation at the low pressures ($< 10^{-4} \text{ dyn/cm}^2$) encountered at these radii.

Figure 2 shows the influence of these dust types on the gas temperature for the M22 model. The gas in outer layers is warmed by about 100 K for dust types A and B. Back-warming isn't significant for any dust type in the layers where most spectral features are formed, which is at temperatures above about 1400 K. Other models showed effects similar to those in this model. In this case, and in most other models, the dust temperatures are higher than the gas temperatures. This provides further justification for assuming that nucleation is complete when grain growth begins. The sharp change in slope of the dotted line at $2.5 R_p$ is due to the the presence of

zero Fe ($x = 1.0$) for smaller radii, and an increasing fraction of Fe at larger radii.

4 OBSERVABLE DUST EFFECTS

The presence of all dust types considered here has a minimal effect on photometry between a wavelength of 1 and $9\ \mu\text{m}$. Near minimum, the J band flux is reduced by 0.1 mag due to extinction by dust for dust types A and B, with no measurable effects on H and K band photometry. However, this small J-band effect is not a reliable model prediction, as it requires growth and destruction rates in the outer layers near minimum that are too high for outer layer pressures $P < 10^{-3}\ \text{dyn/cm}^2$. Up to 0.3 mag extinction for dust type A occurs near-minimum at 900 nm due to back-scattered radiation re-intercepting the lower atmosphere. The extinction of V band light by the dust considered here is too difficult to model, both due to the difficulties in treating strong TiO absorption, and to the influence of the grain size distribution on extinction at short wavelengths.

Interferometric observations at wavelengths short-wards of about $1\ \mu\text{m}$ are sensitive to scattering from dust. Without allowing for significant effects of dust or molecules, larger than expected apparent diameters have led some authors (e.g. Haniff et al. 1995) to favour overtone pulsation for Mira variables. This proposal is clearly in conflict with the now conventional understanding (Wood et al. 1999; Scholz & Wood 2000) that Miras pulsate in the fundamental mode. Note that this discrepancy also existed in the near-infrared (van Belle et al. 1996), but correctly including the effects of molecular contamination of continuum diameters in physical models has since provided a resolution in this case (Woodruff et al. 2004; Fedele et al. 2005). Several authors have clearly mentioned the possibility of dust scattering increasing the apparent size of Mira variables (e.g. Danchi et al. 1994; Hofmann et al. 2001; Ireland et al. 2004d), but a physical model is required to discriminate correctly between the effects of TiO absorption and dust.

Table 3 shows measured diameters of *o* Cet and R Leo from several experiments compared with model predictions of the M22 model with different dust types. The observation phases and targets were: *o* Cet at phases 0.47 and 0.49 (different cycles) for the William Herschel Telescope (WHT) data (Tuthill et al. 1995), *o* Cet at phase 0.34 for the Anglo-Australian Telescope (AAT) data (Ireland et al. 2004d), R Leo at phase 0.2 for the Special Astrophysical Observatory (SAO) data (Hofmann et al. 2001), and R Leo at phase 0.32 from Cambridge Optical Aperture Synthesis Telescope (COAST) (Burns et al. 1998). The COAST data was presented as uniform-disk fits, and the correction factor of 1.52 in the text of Burns et al. (1998) was applied.

For the model fits in Table 3, a least-squared Gaussian fit to visibility V (the normalised Fourier amplitude of the source brightness distribution) was calculated for baselines shorter than where $V = 0.3$. A Gaussian fit was both cited as a better fit than a uniform disk by the authors of the observational papers, and is a better fit in general for the dusty models described here. The model star was placed at 105 pc, in-between the K-band maximum fit distances for R Leo and *o* Cet for the M series Ireland et al. (2004b) and consistent with *Hipparcos* distances. Note that by having models that match the observed temperature as measured by continuum J-K colours (Ireland et al. 2004b) and using the K-band fit distance, the comparison between observed and predicted angular diameters is not heavily dependent on this distance. For example, if the models are under-luminous by 20% with radii 10% too small, then the

model stars will be placed at a distance 10% too close and the predicted angular diameters will remain unchanged.

For the 700, 750 and 920 nm filters, a 20 nm bandwidth was assumed, and for 1045 nm a monochromatic prediction is given. Although these bandwidths did not match the individual experimental bandwidths exactly, the experimental filters all included the chosen wavelengths and would be expected to have similar fit diameters according to the measurements of Ireland et al. (2004d).

It is clear that amongst these models, the observed large diameters and the increase in observed diameter at shorter wavelengths can only be produced by dust A or B, with an intermediate dust being favorable. The scatter in the observations is indicative of both the slightly different phases of observations, and cycle-to-cycle variations in the atmospheric structure. This is also seen in the models, where the fitted FWHMs for the M12 model would be smaller than those for the M22 model.

The wavelengths of 700, 750, 920 and 1045 nm were chosen for this comparison because they are not sensitive to strong TiO absorption in the upper atmosphere. In order to exclude TiO absorption from causing the larger apparent diameters, we have carefully examined the treatment of TiO opacity in our models. The M series spectra have TiO absorption band depths that are much too deep when compared to observations. Although one significant reason for this in the figures of Tej et al. (2003b) was out-dated chemical data for TiO_2 (since replaced with data from Sharp & Huebner 1990), a remaining large problem in modelling the deep absorption bands correctly are non-LTE effects in TiO band formation in a dynamic atmosphere. From the TiO line list of Schwenke (1998), the typical Einstein A coefficient for the upper level in a strong TiO absorption band is $10^7\ \text{s}^{-1}$. This is much higher than the collision rate in the atmospheric regions where the TiO features are formed ($P < 1\ \text{dyn/cm}^2$ and $T < 2000\ \text{K}$). Several simple attempts have been made by us to characterize the magnitude of non-LTE effects. Indeed, spectra with band depths near that observed for typical Miras can be produced by assuming an ad hoc TiO temperature profile. Although these tests affected the strong TiO features significantly, the regions of the spectrum such as those in Table 3 were largely unaffected. This is because these regions of weak and strongly temperature-dependent absorption are formed significantly deeper in the atmosphere than the strong absorption bands. Therefore, we are quite confident that the large apparent diameters can not be caused by TiO alone, and that therefore dust opacity is required to produce the observed diameters.

The Optical Interferometric Polarimetry (OIP) observations of Ireland et al. (2005) are generally consistent with the predictions here. The radii of the dust shells in this paper are approximately $2.5 R_p$, when the model star is placed at the distance corresponding to that which fits the K band maximum. Fitted optical-depths to these observations are between those predicted from the type A and type B dusts. However, the two stars observed in that paper (R Car and RR Sco) have smaller K-band photometric amplitudes than the M-series, and have much less dust emission than *o* Cet or R Leo. Therefore, one might expect the gas densities for these Miras to be smaller than that in the M series at the same radii. This would mean that grain formation and destruction may not be fast compared to the pulsation at the grain formation radii, and would need a more detailed, time-dependent study.

In order to most accurately model the mid-infrared spectra, a new spectrum and intensity profile computation code was constructed. This code used as inputs the gas pressure and molecule partial pressures, the gas and dust temperature and the velocity stratification from the model-construction code. It takes into ac-

Table 3. Model predictions for fitted Gaussian FWHMs to the stellar intensity profile in milli-arcsec for various wavelengths, for the M22 model which is at a phase of 0.37. Measurements for R Leo and *o* Ceti for 4 separate instruments at visual phases between 0.2 and 0.49 are also shown (see text).

| Wavelength (nm) | No Dust | Dust A | Dust B | Dust C | Dust D | WHT | AAT | SAO | COAST |
|-----------------|---------|--------|--------|--------|--------|-----------|-----|------|-------|
| 700 | 22.1 | 50.1 | 27.3 | 22.2 | 23.3 | 27.6/38.2 | 38 | 32.7 | - |
| 750 | 21.8 | 46.9 | 25.6 | 21.8 | 22.7 | - | 32 | 30.5 | - |
| 920 | 22.3 | 37.3 | 24.1 | 22.4 | 22.7 | 23.0 | 23 | - | 29.3 |
| 1045 | 17.8 | 26.7 | 18.7 | 17.8 | 18.1 | - | - | 23.6 | - |

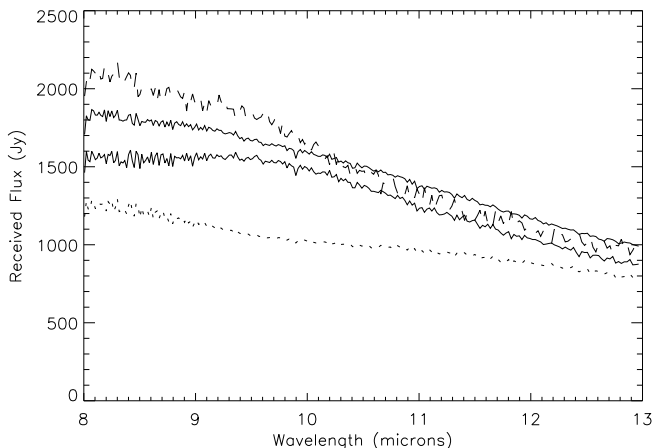


Figure 4. Model spectra for B dust between 8 and 13 microns for the M11n model (lower solid line), M15 model (dotted line), M18 model (dashed line) and M21n model (upper solid line).

count continuum opacities, H_2O lines from Partridge & Schwenke (1997), TiO lines from Schwenke (1998) and other diatomic lines from the input to the ATLAS12 models (Kurucz 1994). The contributions to line profiles from different layers were redshifted or blueshifted as appropriate according to the difference in projected velocities. A micro-turbulence of 2.8 km/s was assumed, in between than used in the M-giant models of Plez et al. (1992) and that derived by Hinkle & Barnes (1979).

The mid-infrared spectra are significantly influenced by dust types A and B, but the spectra for dust types C and D are similar to dust-free models. This is due to the low condensation fraction of dust C at radii where densities are high, and for dust D this is due to the low abundance of Al when compared to Si, Fe and Mg. As dust types A and B result in similar condensation fractions but different grain sizes, their effects on the mid-infrared spectra are very similar. Hence, only selected mid-infrared spectra for representative models with dust B are shown in Figure 4, smoothed to have a resolving power of 500. The model star is placed at a distance of 102 pc, to match the fit distance for the *o* Ceti K-band light curve (Ireland et al. 2004b).

The most crucial point to note about these spectra is that they underestimate the measured flux from *o* Ceti at all wavelengths by a factor of about 2 to 3, based on the range of photometry in Monnier et al. (1998). This is consistent with the measurements of Danchi et al. (1994) and Weiner et al. (2003), whose data require approximately half to three quarters of the total mid-infrared flux from *o* Ceti to originate from a region further from the central star than our model surface (which corresponds to a 58 mas radius at a distance of 102 pc). This dust is almost certainly part of an outflow from this star, and may have a shell-like structure as seen in outflows from other AGB stars (e.g. Hale et al. 1997). Indeed, in

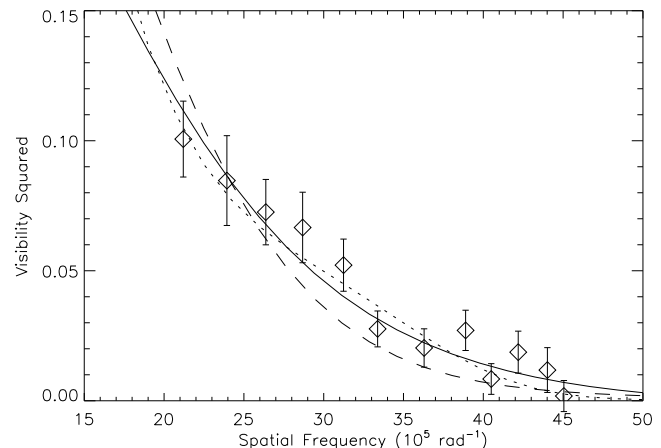


Figure 5. Visibility data used in Weiner et al. (2003) at a pulsation phase of 0.20 (data from November 28, 2000). One-parameter fits (see text) for models at similar phases (see text) are shown for the M11n model (solid line) and the M21n model (dashed line). The dotted line illustrates a three-parameter fit (see text) based on the M21n model and an additional shell of previously ejected dust.

the models a strong shock front occasionally (no more than about 1 cycle in 4) drives a significant amount of mass through the $5 R_p$ surface where it may form part of a stellar wind. Therefore, this additional flux is not inconsistent with the models here, it is simply not part of the models due to the arbitrary $5 R_p$ model surface.

A second important point to note about these model spectra is that they are not well approximated by a black-body spectrum and a silicate emission peak. According to the classification scheme of Sloan & Price (1998), the spectra for the M series with dust B could be classified from SE2 to SE8, with a dust emission contrast of 0.14 to 0.3. This suggests that the observed mid-infrared excess for some Mira variables may not be strictly associated with an outflow (e.g. Ireland et al. 2005).

The effect of these dust types on mid-infrared interferometry is difficult to predict. This is due to the large fraction of the light that originates from dust further than the $5 R_p$ surface to these models (Weiner et al. 2003). Nevertheless, one can say that a general feature of the models is that they do not resemble a uniform-disk intensity profile. Figure 5 shows $11.15 \mu\text{m } V^2$ data from *o* Ceti observations at a phase of 0.2 obtained from J. Weiner (personal communication). This is calibrated data which was used for the model fits in Weiner et al. (2003), unlike the un-calibrated data plotted in Figure 1 of that paper. Intensity profiles were computed using dust B, and the narrow observing bandwidth, assuming a redshift of 83 km/s. Over-plotted in Figure 5 are the model predictions of the M11n model, at a pulsation phase of 0.23, and the predictions of the M21n model at a pulsation phase of 0.22. The model star was placed at the fit distance for the *o* Ceti K-band light curve

(Ireland et al. 2004b) and the fraction of emission from an over-resolved component of extended dust emission was a free parameter. This fraction has the effect of multiplying the squared visibility by a constant smaller than 1.

Certainly in the case of the M11n model the fit is reasonable, and the 45 % additional flux required from extended dust emission is roughly consistent with observed mid-infrared excesses for *o* Cet. In the case of the M21 model, additional model parameters would be required to fit the data reasonably. The example plotted as the dotted line is one where two additional parameters were free: the radius of an additional shell of dust and the fractional emission from this shell. The parameters for this model were a dust shell radius of $5.83 R_p$ containing 18 % of the total emission. This demonstrates that for mid-infrared interferometry to provide accurate constraints on the innermost dust and water emission, a model or observations of dust at large radii must be combined with models of the inner regions as described here. Examining data from several other epochs did not give significant errors when fitting dust B models to the data, but dust-free models were not in general extended enough to fit the data from Weiner et al. (2003).

A final observable feature of the dust formation models as described here is the phase- and cycle-dependence of the dust formation. A relatively quick increase in dust opacity is predicted near minimum during certain cycles wherever a shock front passes through the radius of dust formation. This occurs around phase 1.4 in these models, where the $1.04 \mu\text{m}$ dust optical depth rapidly increases from 0.26 to 0.72 for dust A. This increase in opacity would be best seen interferometrically by a jump in size at either wavelengths short-wards of $1 \mu\text{m}$ or in the mid-infrared. Combined observations at these two wavelength regimes could constrain grain sizes (e.g. the difference between dust types A and B).

The cycle-dependence of the outer layers in the M and P series relates to their chaotic nature. There is no reason to expect these layers to show high degrees of spherical symmetry as assumed in the models. A crude approximation is that one could think of opposite sides of a star to be in different model ‘cycles’. Similar behaviour is evident on large scales in the models of Woitke (2005). For this reason, dust formation near-minimum may also be observable as the creation of asymmetric features in a shell at $2-3 R_p$. One effect of this dust creation would be rapid changes in the angle of polarization observed. This effect is a plausible explanation for the rapid changes in polarization angle observed around Julian day 2441000 (near phase 0.5) for R Leo by Serkowski & Shawl (2001). These observations show polarizations of several percent in U, B and V bands where the angle of polarization changes by 25 degrees in one direction over 50 days, then 50 degrees in the opposite direction over the following 50 days.

5 CONCLUSION

Condensation of corundum and silicate dust in a model of a $1.2 M_\odot$ self-excited Mira variable has been examined. Four dust types were modelled, representing approximated physical dust formation parameters. It was found that a dust type between A and B from Table 1 fits existing observations well ¹. In particular, the effect of scattering by this type of dust explains the systematically large observed apparent diameters at wavelengths shorter than $1 \mu\text{m}$. This

dust type has approximately 10^{-13} grain nuclei per H atom available at the onset of silicate condensation, and requires α , the ratio of the exchange coefficient for Mg and Fe ion to the sticking coefficient of SiO, to be at least the order of unity. A model where only corundum forms was found to be a poor fit to observations of *o* Cet and R Leo. The use of composition-dependent opacities enabled the survival of the initial Mg-rich silicate condensate at radii of 2-3 times the model parent star radius.

ACKNOWLEDGMENTS

This research was supported by the Australian Research Council and the Deutsche Forschungsgemeinschaft within the linkage project ‘‘Red Giants’’, and by a grant of the Deutsche Forschungsgemeinschaft on ‘‘Time Dependence of Mira Atmospheres’’. We would like to thank P. G. Tuthill and the referee P. Woitke for valuable comments on the manuscript, and H. P. Gail for answering many questions about dust formation theory.

REFERENCES

- Balducci G., Gigli G., Guido M., 1985, *J. Chem. Phys.*, 83, 1909
 Bedding T. R., Jacob A. P., Scholz M., Wood P. R., 2001, *MNRAS*, 325, 1487
 Burns D., Baldwin J. E., Boysen R. C., Haniff C. A., Lawson P. R., Mackay C. D., Rogers J., Scott T. R., St.-Jacques D., Warner P. J., Wilson D. M. A., Young J. S., 1998, *MNRAS*, 297, 462
 Danchi W. C., Bester M., 1995, *Ap&SS*, 224, 339
 Danchi W. C., Bester M., Degiacomi C. G., Greenhill L. J., Townes C. H., 1994, *AJ*, 107, 1469
 Dorschner J., Begemann B., Henning T., Jaeger C., Mutschke H., 1995, *A&A*, 300, 503
 Egan M. P., Sloan G. C., 2001, *ApJ*, 558, 165
 Fedele D., Wittkowski M., Paresce F., Scholz M., Wood P. R., Ciroti S., 2005, *A&A*, 431, 1019
 Gail H.-P., 2003, in *LNP Vol. 609: Astromineralogy*, Th. Henning ed., Vol. 609, p. 55
 Gail H.-P., Sedlmayr E., 1999, *A&A*, 347, 594
 Gauger A., Sedlmayr E., Gail H.-P., 1990, *A&A*, 235, 345
 Gautschy-Loidl R., Höfner S., Jørgensen U. G., Hron J., 2004, *A&A*, 422, 289
 Höfner S., Gautschy-Loidl R., Aringer B., Jørgensen U. G., 2003, *A&A*, 399, 589
 Hale D. D. S., Bester M., Danchi W. C., Hoss S., Lipman E., Monnier J. D., Tuthill P. G., Townes C. H., Johnson M., Lopez B., Geballe T. R., 1997, *ApJ*, 490, 407
 Haniff C. A., Scholz M., Tuthill P. G., 1995, *MNRAS*, 276, 640
 Harman A. K., Ninomiya S., Adachi S., 1994, *Journal of Applied Physics*, 76, 8032
 Harris L., 1955, *Journal of the Optical Society of America* (1917-1983), 45, 27
 Helling C., Winters J. M., Sedlmayr E., 2000, *A&A*, 358, 651
 Hinkle K. H., Barnes T. G., 1979, *ApJ*, 227, 923
 Hofmann K.-H., Balega Y., Scholz M., Weigelt G., 2001, *A&A*, 376, 518
 Hofmann K.-H., Scholz M., Wood P. R., 1998, *A&A*, 339, 846
 Ireland M., Tuthill P., Robertson G., Bedding T., Jacob A., Monnier J., Danchi W., 2004a, in *ASP Conf. Ser. 310: IAU Colloq. 193: Variable Stars in the Local Group*, p. 327

¹ Predictions of existing and additional models are available upon request to anyone interested for specific observational programs.

- Ireland M. J., Scholz M., Tuthill P. G., Wood P. R., 2004b, *MNRAS*, 355, 444
- Ireland M. J., Scholz M., Wood P. R., 2004c, *MNRAS*, 352, 318
- Ireland M. J., Tuthill P. G., Bedding T. R., Robertson J. G., Jacob A. P., 2004d, *MNRAS*, 350, 365
- Ireland M. J., Tuthill P. G., Davis J., Tango W., 2005, *MNRAS*, 361, 337
- Jäger C., Dorschner J., Mutschke H., Posch T., Henning T., 2003, *A&A*, 408, 193
- Jacob A. P., Scholz M., 2002, *MNRAS*, 336, 1377
- Jeong K. S., Chang C., Sedlmayr E., Sülze, 2000, *J. Phys.B*, 33, 3417
- Jeong K. S., Winters J. M., Le Bertre T., Sedlmayr E., 2003, *A&A*, 407, 191
- Koike C., Kaito C., Yamamoto T., Shibai H., Kimura S., Suto H., 1995, *Icarus*, 114, 203
- Kurucz R. L., 1994, in *LNP Vol. 428: IAU Colloq. 146: Molecules in the Stellar Environment*, Jørgensen, U.G. ed., Vol. 428, p. 282
- Lopez B., Danchi W. C., Bester M., Hale D. D. S., Lipman E. A., Monnier J. D., Tuthill P. G., Townes C. H., Degiacomi C. G., Geballe T. R., Greenhill L. J., Cruzalebes P., Lefevre J., Mekarina D., Mattei J. A., Nishimoto D., Kervin P. W., 1997, *ApJ*, 488, 807
- Maldoni M. M., Ireland T. R., Smith R. G., Robinson G., 2005, *MNRAS*, 362, 872
- Monnier J. D., Geballe T. R., Danchi W. C., 1998, *ApJ*, 502, 833
- Monnier J. D., Millan-Gabet R., Tuthill P. G., Traub W. A., Carleton N. P., Coudé du Foresto V., Danchi W. C., Lacasse M. G., Morel S., Perrin G., Porro I. L., Schloerb F. P., Townes C. H., 2004, *ApJ*, 605, 436
- Ohnaka K., 2004, *A&A*, 424, 1011
- Ohnaka K., Bergeat J., Driebe T., Graser U., Hofmann K.-H., Köhler R., Leinert C., Lopez B., Malbet F., Morel S., Paresce F., Perrin G., Preibisch T., Richichi A., Schertl D., Schöller M., Sol H., Weigelt G., Wittkowski M., 2005, *A&A*, 429, 1057
- Ozawa K., Nagahara H., 2000, *Geochim. Cosmochim. Acta*, 64, 939
- Palme H., Suess H. E., Zeh H. D., 1981, in: Voigt H.H., Schaifers K. (eds) *Landolt-Börnstein, Numerical Data and Functional Relationships in Science and Technology*, Vol. VI/2a, Springer, Berlin Heidelberg New York, p. 257
- Partridge H., Schwenke D. W., 1997, *J. Chem. Phys.*, 106, 4618
- Perrin G., Ridgway S. T., Mennesson B., Cotton W. D., Woillez J., Verhoelst T., Schuller P., Coudé du Foresto V., Traub W. A., Millan-Gabet R., Lacasse M. G., 2004, *A&A*, 426, 279
- Plez B., Brett J. M., Nordlund A., 1992, *A&A*, 256, 551
- Schirmmacher V., Woitke P., Sedlmayr E., 2003, *A&A*, 404, 267
- Scholz M., Wood P. R., 2000, *A&A*, 362, 1065
- Schwenke D. W., 1998, in *Chemistry and Physics of Molecules and Grains in Space*. *Faraday Discussions* No. 109, p. 321
- Serkowski K., Shawl S. J., 2001, *AJ*, 122, 2017
- Sharp C. M., Huebner W. F., 1990, *ApJS*, 72, 417
- Sloan G. C., Price S. D., 1998, *ApJS*, 119, 141
- Tej A., Lançon A., Scholz M., 2003a, *A&A*, 401, 347
- Tej A., Lançon A., Scholz M., Wood P. R., 2003b, *A&A*, 412, 481
- Tuthill P. G., Haniff C. A., Baldwin J. E., 1995, *MNRAS*, 277, 1541
- van Belle G. T., Dyck H. M., Benson J. A., Lacasse M. G., 1996, *AJ*, 112, 2147
- Weiner J., Hale D. D. S., Townes C. H., 2003, *ApJ*, 588, 1064
- Winters J. M., Le Bertre T., Jeong K. S., Helling C., Sedlmayr E., 2000, *A&A*, 361, 641
- Woitke P., 2005, *A&A*, Submitted
- Woitke P., Helling C., Winters J. M., Jeong K. S., 1999, *A&A*, 348, L17
- Wood P. R., Alcock C., Allsman R. A., Alves D., Axelrod T. S., Becker A. C., Bennett D. P., Cook K. H., Drake A. J., Freeman K. C., Griest K., King L. J., Lehner M. J., Marshall S. L., Minniti D., Peterson B. A., Pratt M. R., Quinn P. J., Stubbs C. W., Sutherland W., Tomaney A., Vandehei T., Welch D. L., 1999, in *IAU Symp. 191: Asymptotic Giant Branch Stars*, p. 151
- Woodruff H. C., Eberhardt M., Driebe T., Hofmann K.-H., Ohnaka K., Richichi A., Schertl D., Schöller M., Scholz M., Weigelt G., Wittkowski M., Wood P. R., 2004, *A&A*, 421, 703